Low temperature synthesis of garnet solid state electrolytes

Dong, Bo; Driscoll, Laura; Stockham, Mark; Kendrick, Emma; Slater, Peter

DOI:
10.1016/j.ssi.2020.115317

Document Version
Peer reviewed version

Citation for published version (Harvard):
Dong, B, Driscoll, L, Stockham, M, Kendrick, E & Slater, P 2020, 'Low temperature synthesis of garnet solid state electrolytes: implications on aluminium incorporation in $Li_7La_3Zr_2O_{12}$', *Solid State Ionics*, vol. 350, 115317. https://doi.org/10.1016/j.ssi.2020.115317

Low temperature synthesis of garnet solid state electrolytes: implications on aluminium incorporation in $Li_7La_3Zr_2O_{12}$

Bo Dong[†,], Laura L. Driscoll[†], Mark P. Stockham[†], Emma Kendrick[‡], Peter R. Slater[†,*]*

†School of Chemistry, University of Birmingham, B15 2TT, UK

‡School of Metallurgy and Materials, University of Birmingham, B15 2TT, UK

*b.dong@bham.ac.uk; p.r.slater@bham.ac.uk;

Abstract

Li ion conducting garnet electrolytes are attracting considerable interest for potential use in all solid state batteries. Nevertheless, their synthesis can be challenging due to the high temperatures required leading to significant Li loss, and consequently the need to add excess Li to counteract this. In this work, we report a low temperature biopolymer sol-gel route to synthesise these garnet materials using Agar (to ensure homogeneous mixing and nucleation through this biotemplating matrix), with the formation of the garnet phase starting at temperatures as low as 600 ^{o}C, with single phase samples of tetragonal $Li_7La_3Zr_2O_{12}$, and cubic $Li_{6.4}Al_{0.2}La_3Zr_2O_{12}$ prepared at 700 ^{o}C (~ 400 ^{o}C lower than the conventional solid state routes). Significantly, this route also allowed the synthesis of these garnets without the need for Li excess for the first time, due to the low temperature limiting Li loss. Moreover, if Li excess was used in the synthesis of cubic $Li_{6.4}Al_{0.2}La_3Zr_2O_{12}$, Al incorporation was not observed at this temperature, and rather tetragonal $Li_7La_3Zr_2O_{12}$ was obtained. Contrary to previous assumptions, this indicates that the Li is more stable in the structure than Al at low temperature. Thus, Al incorporation only occurs if there is a deficiency of Li in the starting material, or if the sample is heated to elevated temperatures to induce Li volatility, so as to drive the incorporation of Al to charge balance the resultant Li loss.

Introduction

Lithium ion batteries (LIBs) revolutionised the growth of portable electronics due to their high power and energy densities, and long term durability[1-3]. Nowadays, the LIB market has begun to concentrate on electric vehicle (EV) applications, which not only require higher energy densities but, more importantly, improved safety over a wide range of temperature[4]. In this respect, organic electrolytes used in LIBs are flammable and may thus cause safety issues, making it a non-ideal system for EVs. All-Solid-State Batteries (ASSBs) which replace the organic electrolyte by a solid state electrolyte (SSE) are being considered as next generation batteries for such applications due to their enhanced safety properties[5, 6]. The ideal SSE should have a wide electrochemical stability window, high Li^+ ion conductivity, negligible electronic conductivity, high mechanical strength, environmental friendliness and low cost. To date, a large family of SSEs have been investigated, including LISICON, Thio-LISICON, NASICON, Perovskite, garnet, argyrodite, anti-perovskite amongst others[7-14]. Considering the combination of good electrochemical stability and high Li^+ ionic conductivity, the garnet system is deemed as a promising candidate for ASSBs[15-17].

Ideal garnets have a general formula $A_3B_2C_3O_{12}$ where A, B and C are 8, 6 and 4 oxygen coordinated metal ions. The crystal structure of garnet contains a framework of corner-linked tetrahedra and octahedra with the A cations sitting in the cavities. The first fast Li^+ ion conducting garnet, $La_3M_2Li_5O_{12}$ (M =

Nb, Ta), was reported in 2003 by Thangadurai et al[18-20]. Structural studies have shown that the lithium content and the distribution of lithium ions in the structure is strongly related to the conductivity and lithium diffusion pathway in the garnet[21]. Subsequently, the stoichiometric tetragonal $Li_7La_3Zr_2O_{12}$ (LLZO) phase, as well as Sn, Hf based analogues, with the maximum lithium content in the garnet structure were reported, where lithium ions are ordered in three fully occupied sites (tetrahedral 8a and octahedral 16f and 32g sites). This Li ordering leads to a low Li ionic conductivity[22-25]. High temperature X-ray diffraction shows that undoped $Li_7La_3Zr_2O_{12}$ displays a reversible tetragonal – cubic phase transition at 750 ^oC. However room temperature cubic phases, with high conductivity, can be stabilised through incorporation with aluminium from a reaction with alumina crucibles (1 Al^{3+} replaces 3 Li^+), or proton – lithium exchange from atomospheric moisture[26-29]. Multiple aliovalent doping strategies have been applied to enhance the conductivity of LLZO, and the optimum conductivity in these garnet systems is demonstrated for lithium contents of 6.4 – 6.6 per formula unit[30-41]. Nowadays, the electrolyte-electrode interfacial issues have attracted a great attention, as this remains the primary barrier to their practical application. An insulating Li_2CO_3 layer usually forms in humid atmosphere due to H^+/Li^+ exchange, which is demonstrated to be effectively removed through mechanical polishing inside a glove box[42]. Both metal or non-metal coating and consequently alloying with Li metal, and polymer – garnet composite systems have been applied to try to decrease the

high interfacial resistance and limit dendrite growth through the garnet electrolyte[43-50].

A wide range of synthetic methods, such as solid state and sol-gel approaches, have also been used to synthesise garnet solid state electrolyte materials; however, most involve a high reaction temperature, ~ 900 – 1200 ^{o}C, which not only leads to lithium evaporation issues, but also high energy cost during the synthesis[51-54]. In this work, we have investigated a biopolymer complexation approach to synthesise these garnets in an attempt to lower the synthesis temperature to allow synthesis without Li excess. A comparison of the synthesis routes of $Li_7La_3Zr_2O_{12}$ is shown in table 1. Biopolymers contain large numbers of functional groups which create negative chelation sites (giving a flexible metal coordination matrix) when dissolved in water. This matrix subsequently 'traps' metal cations from solution and allows the formation of a homogeneous aqueous gel, which acts as a precursor for sol-gel synthesis (see the biopolymer review[55]). The process promotes nano-sized particle formation at reduced temperatures compared to that of traditional solid state methods, with the biotemplate removed by the thermal treatment[56].

One particular biopolymer example is Agar, which is made of a mixture of agarose and agaropectin, as shown in figure 1. It has been widely used in the food industry and microbiological field; e.g. thickeners for fruit preserves, ice cream and other desserts, appetite suppressants and a vegetarian substitute

for gelatin. Here, we show that this low-cost biopolymer can be used to synthesise the garnet solid-state electrolyte materials. Both stoichiometric $Li_7La_3Zr_2O_{12}$ and Al doped $Li_7La_3Zr_2O_{12}$ can be made at 700 ^oC, which is about ~ 400 ^oC lower than the conventional solid state route, and the results raise interesting questions regarding Al incorporation in conventional solid state synthesis. Moreover, through addition of LiF as a sintering aid, dense garnet membranes with high conductivity can be obtained at 1100 ^oC/4h in air (lower than >1200 ^oC typically used). The long-term cycling of a Li//$Li_{6.4}Al_{0.2}La_3Zr_2O_{12}$//Li cell using samples made via this route was demonstrated over 210 hours.

Experimental

Synthesis of $Li_7La_3Zr_2O_{12}$, and $Li_{7-3x}Al_xLa_3Zr_2O_{12}$

$LiNO_3$, $ZrO(NO_3)_2{\cdot}xH_2O$ (x = 1.4, from TGA analysis), $La(NO_3)_3{\cdot}6H_2O$, $Al(NO_3)_3{\cdot}9H_2O$ and Agar biopolymer were chosen as starting materials. $ZrO(NO_3)_2{\cdot}xH_2O$ was added to the dilute nitric acid (different concentrations of 0.1, 0.25, 0.5, 1, 2 M were investigated), heated to 80 ^oC and stirred until full dissolution of $ZrO(NO_3)_2{\cdot}xH_2O$. Stoichiometric amounts of $LiNO_3$, $La(NO_3)_3{\cdot}6H_2O$, $Al(NO_3)_3{\cdot}9H_2O$, and 10% excess $LiNO_3$ (to compensate the lithium loss during the synthesis) were added to the same solution and mixed for 30 mins. Agar (5 wt%) was then added to the solution which was stirred for an hour before transferring to an oven and drying at 100 °C. The resultant precursor was heated to 350 °C at a 0.5 °C min^{-1} heating rate to slowly

decompose the matrix and allow the garnet nucleation. Finally, the sample was reground and heated at ~ 700 - 800 °C for 12 hours at a 10 ^{o}C min^{-1} heating rate to gain the final product.

Characterisation of Materials

X-ray diffraction (XRD) data were collected using a Bruker D8 X-ray diffractometer with linear position sensitive detector (PSD) (CuKα radiation). Patterns were recorded over 2θ range 10^{o} to 60^{o} with a 0.02^{o} step size.

Variable temperature X-ray (VTXRD) data were collected on a Bruker D8 variable temperature X-ray diffractometer with a linear position sensitive detector (CuKα radiation) and an Anton Parr heating stage. A flat holder was used for sample preparation, and VTXRD data of the heated precursor mixture were collected between 350 ^{o}C and 800 ^{o}C with 50 ^{o}C interval steps for 30 minutes in order to determine an approximate temperature for the garnet formation.

The microstructure was assessed by scanning electron microscopy using a HITACHI TM4000plus SEM. An energy dispersive X-ray spectroscopy (EDX) detector from AztecOne was used to probe the distribution of elements of sample.

Pellets (9.8 mm diameter) for conductivity were prepared by adding 2 wt% LiF^{57} as a sintering aid, pressing at 0.2 tons and sintering aid at 1100 ^{o}C at a heating rate of 5 ^{o}Cmin^{-1} for 4 h in air (The pellet was covered with sacrificial powder from the same batch to prevent the lithium loss during the heating

process). After sintering, both sides of the pellet were painted with Au paste and heated at 850 ^{o}C for 1 hour. A HP 4192 analyser was used to record the impedance data with 100 mV applied ac voltage over the frequency range 1 to 10^{7} Hz.

Cell assembly and electrochemical characterisation

Both sides of the $Li_{6.4}Al_{0.2}La_3Zr_2O_{12}$ pellet were polished in a dry room and coated with thin layer of sputtered Au for enhanced electrical contact. Li//$Li_{6.4}Al_{0.2}La_3Zr_2O_{12}$//Li symmetric cell was hot pressed for 1 hour at 175 ^{o}C and assembled using a swagelok cell in an Argon filled glove box. Electrochemical impedance spectroscopy (EIS) was conducted using a Solatron 1260 analyser at 100 mV over the frequency range from 0.1 to 10^{7} Hz. The plating/stripping property was characterised with a Bio-logic SP50 cell tester (see supplementary info for cell test results).

Results and discussion

Phase formation

As shown in figure 2a, initial experiments showed higher quality XRD patterns for samples made with agar compared to those without agar under the same conditions (700°C/12h). However, for the initial experiments which utilised 2M HNO_3 to dissolve the $ZrO(NO_3)_2{\cdot}xH_2O$, La_2O_3 is still present in the sample made with agar. This may be associated with partial decomposition of the agar by the harsh acidic conditions. In order to optimise the synthesis of $Li_7La_3Zr_2O_{12}$ through this biopolymer route, lower nitric acid concentrations,

0.1M, 0.25M, 0.5M, 1M, were therefore studied (figure 2b). These showed that the acidity of the solution needs to be sufficiently high to aid the dissolution of $ZrO(NO_3)_2 \cdot xH_2O$, but also not too strong to decompose the agar template. From these studies, 0.5M HNO_3 concentration was shown to be the optimum.

The morphology of $Li_{6.4}Al_{0.2}La_3Zr_2O_{12}$ prepared with and without Agar at 700 ^oC is shown in figure 2c. A distinct morphology with smaller particle size within a 3D homogeneous biotemplate matrix was observed from the sample made with Agar, while particle aggregation and irregular particle distribution were seen for the sample synthesised without Agar. This shows the benefit of agar in assisting the synthesis of the garnet phase leading to the prevention of agglomeration as well as avoiding the creation of intermediate products by the biotemplate matrix.

VTXRD was used to determine the lowest possible temperature to form $Li_7La_3Zr_2O_{12}$. Figure 3a shows the mixture is still an amorphous phase at 350 ^oC but that the $Li_7La_3Zr_2O_{12}$ garnet starts to form at temperatures as low as 600 ^oC. As shown in figure 4a, complete formation of tetragonal $Li_7La_3Zr_2O_{12}$ was observed in the sample made through the biotemplating route at 700 °C/12h, which is ~400 ^oC lower than the conventional solid state methods. We believe that this dramatic temperature decrease is due to a more homogeneous metal ion mixing and garnet nucleation through the formation of the biotemplating matrix. While we do not have direct evidence for this homogeneous garnet nucleation in the process, SEM and EDX (figure 4b) analysis of the resultant

phases shows a homogeneous distribution of La, Zr, Al and O within $Li_{6.4}Al_{0.2}La_3Zr_2O_{12}$ sample, which suggests that this may be the case and further supports that this method is an effective way in synthesising garnet solid state electrolyte materials at low temperatures.

A common issue in making garnet is lithium evaporation during high temperature synthesis, so excess lithium (typically >20%) needs to be added to compensate for that loss. In order to determine whether the lower temperature agar method eliminated this problem, we also investigated the synthesis without Li excess. This work showed no Li excess was needed, with formation of a single phase $Li_7La_3Zr_2O_{12}$ at 700°C for stoichiometric Li contents. Moreover, similar results were observed for the synthesis of Al doped garnets; the results showing that single phase cubic $Li_{6.55}Al_{0.15}La_3Zr_2O_{12}$ could be prepared at 700 ^oC without Li excess (figure 5). Interestingly for this Al doped sample, the addition of 10% excess Li led to the formation of a tetragonal garnet phase (figure 5), suggesting no Al incorporation into $Li_7La_3Zr_2O_{12}$. Contrary to previous assumptions, this result therefore suggests that the replacement of Li by Al is thermodynamically unfavourable and only occurs when there is a deficiency of Li to act as a driving force for the incorporation. In agreement with this, the 10% Li excess $Li_{6.55}Al_{0.15}La_3Zr_2O_{12}$ samples sintered at 1100°C showed the formation of a single cubic garnet phase, as Li loss at elevated temperatures allowed the incorporation of Al. The sample without Li excess also maintained the cubic garnet phase on sintering at 1100°C, but in

this case small impurities (ZrO_2, Al_2O_3) were observed due to Li loss. Thus, Li excess is not needed to produce the pure garnet phase at 700°C but is required for the final sintering at elevated temperatures to produce a dense pellet. This result has significant implications for Al doped garnet phases, which are widely utilised in the literature. In particular, Al incorporation only appears to occur if there is a deficiency of Li in the starting material, or if the sample is heated to elevated temperatures to induce Li volatility, so as to drive the incorporation of Al to charge balance the resultant Li loss. Thus, it is likely that normal high temperature synthesis/sintering of Al doped $Li_7La_3Zr_2O_{12}$ leads to inhomogeneity on Al incorporation throughout the sample as well as within individual grains, dependent on the level of Li loss[58, 59]. This result may then help to explain some of the wide variation in garnet conductivities in the literature, as well as the challenges in utilizing these electrolytes in solid state cells.

Furthermore, if new lower temperature cold sintering, or field assisted sintering of these garnets can be optimized, then this route offers an important avenue to prepare low temperature (no Li excess) homogeneous samples, which are likely to present optimum conducting properties using such low temperature sintering processes[60].

Conductivity results

The conductivity of $Li_{6.4}Al_{0.2}La_3Zr_2O_{12}$ (10% excess Li) prepared by this biopolymer route was then investigated. Pellets were prepared with and

without LiF sintering aid. XRD data for both sintered samples showed a single phase cubic garnet phase, although the sample sintered at 1100°C without LiF addition was much less dense (65% versus 81%), and resulted in lower conductivity. The Impedance complex plane Z* plot of LiF- $Li_{6.4}Al_{0.2}La_3Zr_2O_{12}$ with Au paste electrodes is shown in figure 6a. Two semicircles at high and intermediate frequencies, and a spike at low frequency are observed. Figure 9 shows the circuit fitting of Z* plot, where a parallel resistor (R1) and constant phase element (CPE1) in series with another parallel resistor (R2) and constant phase element (CPE2) were used to fit the first and second semicircles. The low frequency spike corresponds to a CPE3 which is in series with R1/CPE1 and R2/CPE2.

The capacitance (C') was observed as a function of frequency is shown in figure 6b. A plateau with value of 6 x 10^{-12} Fcm^{-1} at higher frequency with associated bulk permittivity of 67 calculated from $\varepsilon_{\infty'} = C/\varepsilon_0$, where ε_0 is the permittivity of free space with a value of 8.854×10^{-14} F cm^{-1}. An intermediate plateau with value of 10^{-10} Fcm^{-1} at intermediate frequency was seen, which is a typical value for grain boundary response[61]. At the lower frequency, part of a third plateau with a capacitance of 10^{-6} Fcm^{-1} was seen, which indicates the sample – electrode interface response and a double layer phenomenon; herein, Li^+ ion conduction.

The conductivity (Y') versus frequency plot (figure 6c) shows two frequency independent plateaus at intermediate frequency, which are attributed to the

bulk and grain boundary responses. A dispersion at low frequency is detected, which represents the Li^+ ion blocking at the sample – electrode interface. Additionally, a curvature associated with the Jonscher's power law was observed at high frequency[62].

The Arrhenius plot of LiF- $Li_{6.4}Al_{0.2}La_3Zr_2O_{12}$ is shown in figure 7. The bulk and total conductivities reach 1 x 10^{-4} Scm^{-1} at room temperature with an activation energy of 0.29 eV in the temperature range 50 – 125 ^oC, which are comparable to samples prepared and sintered at high temperature in the literature.

Conclusions

A low temperature biotemplating sol-gel route to synthesise garnet materials using Agar polymer was shown. Tetragonal $Li_7La_3Zr_2O_{12}$, and cubic $Li_{6.4}Al_{0.2}La_3Zr_2O_{12}$ were made successfully at 700 ^oC, which is ~ 400 ^oC lower than the conventional solid state routes. Significantly, this route also allowed the synthesis of these garnets without the need for Li excess for the first time, although excess Li was required to balance Li loss on subsequent high temperature sintering. Such sintered garnets showed high conductivities and the long-term cycling of a Li//$Li_{6.4}Al_{0.2}La_3Zr_2O_{12}$//Li cell was demonstrated over 210 hours (see supplementary information). The synthesis work also suggests that, contrary to previous assumptions, Li is more stable in the structure than Al. Thus Al incorporation only occurs if there is a deficiency of Li in the starting material, or if the sample is heated to elevated temperatures to induce Li

volatility, so as to drive the incorporation of Al to charge balance the resultant Li loss.

Acknowledgements

We would like to thank EPSRC (grant EP/R024006/1, and EP/P033822/1), the APC (GEM: Garnet Electrolyte Manufacture 56065), and the University of Birmingham (Studentship for MPS) for financial support.

Conflict of Interest

The authors declare no conflict of interest.

Reference

1. Tarascon, J.-M.; Armand, M., Issues and Challenges Facing Rechargeable Lithium Batteries. *Nature.* **2001,** 414, 359.

2. Bruce, P. G.; Scrosati, B.; Tarascon, J. M., Nanomaterials for Rechargeable Lithium Batteries. *Angew. Chem. Int. Ed.* **2008,** 47, (16), 2930-46.

3. Goodenough, J. B.; Park, K. S., The Li-Ion Rechargeable Battery: A Perspective. *J. Am. Chem. Soc.* **2013,** 135, (4), 1167-76.

4. Larcher, D.; Tarascon, J. M., Towards Greener and More Sustainable Batteries for Electrical Energy Storage. *Nat. Chem.* **2015,** 7, (1), 19-29.

5. Janek, J.; Zeier, W. G., A Solid Future for Battery Development. *Nat. Energy* **2016,** 1, (9).

6. Zheng, F.; Kotobuki, M.; Song, S.; Lai, M. O.; Lu, L., Review on Solid

Electrolytes for All-Solid-State Lithium-Ion Batteries. *J. Power Sources.* **2018,** 389, 198-213.

7. Bruce, P. G.; West, A. R., The A-C Conductivity of Polycrystalline LISICON, $Li_{2+2X}Zn_{1-x}GeO_4$, and a Model for Intergranular Constriction Resistances. *J. Electrochem. Soc.* **1983,** 130.

8. M.A. Subramanian; R. Subramanian; A. Clearfield, Lithium Ion Conductors in the System $AB(IV)_2(PO_4)_3$ (B = Ti, Zr and Hf). *Solid State Ionics.* **1986,** 18, 562.

9. Y. Harada; T. Ishigaki; H. Kawai; Kuwano, J., Lithium Ion Conductivity of Polycrystalline Perovskite $La_{0.67-x}Li_{3x}TiO_3$ with Ordered and Disordered Arrangements of the A-Site Ions. *Solid State Ionics.* **1998,** 108, 407.

10. V. Thangadurai; A.K. Shukla; Gopalakrishnan, J., New Lithium-Ion Conductors Based on the NASICON Structure. *J. Mater. Chem.* **1999,** 9, 739.

11. Kanno, R.; Murayama, M., Lithium Ionic Conductor Thio-LISICON the Li_2S-GeS_2-P_2S_5 System. *J. Electrochem. Soc.* **2001,** 148.

12. Dong, B.; Jarkaneh, R.; Hull, S.; Reeves-McLaren, N.; Biendicho, J. J.; West, A. R., Synthesis, Structure and Electrical Properties of N-doped Li_3VO_4. *J. Mater. Chem. A.* **2016,** 4, (4), 1408-1413.

13. Huang, X.; Lu, Y.; Jin, J.; Gu, S.; Xiu, T.; Song, Z.; Badding, M. E.; Wen, Z., Method Using Water-Based Solvent to Prepare $Li_7La_3Zr_2O_{12}$ Solid Electrolytes. *ACS Appl. Mater. Interfaces.* **2018,** 10, (20), 17147-17155.

14. Dong, B.; Yan, J.; Walkley, B.; Inglis, K. K.; Blanc, F.; Hull, S.; West, A. R.,

Synthesis and Characterisation of the New Oxyfluoride Li^+ Ion Conductor, Li_5SiO_4F. *Solid State Ionics.* **2018,** 327, 64-70.

15. Thangadurai, V.; Narayanan, S.; Pinzaru, D., Garnet-Type Solid-State Fast Li Ion Conductors for Li Batteries: Critical Review. *Chem. Soc. Rev.* **2014,** 43, (13), 4714-27.

16. Ramakumar, S.; Deviannapoorani, C.; Dhivya, L.; Shankar, L. S.; Murugan, R., Lithium Garnets: Synthesis, Structure, Li^+ Conductivity, Li^+ Dynamics and Applications. *Prog. Mater. Sci.* **2017,** 88, 325-411.

17. Sun, C.; Liu, J.; Gong, Y.; Wilkinson, D. P.; Zhang, J., Recent Advances in All-Solid-State Rechargeable Lithium Batteries. *Nano Energy.* **2017,** 33, 363-386.

18. Thangadurai, V.; Kaack, H.; Weppner, W., Novel Fast Lithium Ion Conduction in Garnet-Type $Li_5La_3M_2O_{12}$ (M = Nb, Ta). *J. Am. Ceram. Soc.* **2003,** 86, 437.

19. Thangadurai, V.; Adams, S.; Weppner, W., Crystal Structure Revision and Identification of Li+-Ion Migration Pathways in the Garnet-like $Li_5La_3M_2O_{12}$ (M = Nb, Ta) Oxides. *Chem. Mater.* **2004,** 16, 2998.

20. Cussen, E. J., The Structure of Lithium Garnets: Cation Disorder and Clustering in A New Family of Fast Li^+ Conductors. *Chem. Commun.* **2006**, (4), 412-413.

21. Cussen, E. J., Structure and Ionic Conductivity in Lithium Garnets. *J. Mater. Chem.* **2010,** 20, (25).

22. Murugan, R.; Thangadurai, V.; Weppner, W., Fast Lithium Ion Conduction in Garnet-Type $Li_7La_3Zr_2O_{12}$. *Angew. Chem. Int. Ed.* **2007,** 46, (41), 7778-81.

23. Awaka, J.; Kijima, N.; Hayakawa, H.; Akimoto, J., Synthesis and Structure Analysis of Tetragonal $Li_7La_3Zr_2O_{12}$ with the Garnet-Related Type Structure. *J. Solid State Chem.* **2009,** 182, (8), 2046-2052.

24. Percival, J.; Kendrick, E.; Smith, R. I.; Slater, P. R., Cation Ordering in Li Containing Garnets: Synthesis and Structural Characterisation of the Tetragonal System, $Li_7La_3Sn_2O_{12}$. *Dalton Trans.* **2009**, (26), 5177-5181.

25. Awaka, J.; Kijima, N.; Kataoka, K.; Hayakawa, H.; Ohshima, K.-i.; Akimoto, J., Neutron Powder Diffraction Study of Tetragonal $Li_7La_3Hf_2O_{12}$ with the Garnet-Related Type Structure. *J. Solid State Chem.* **2010,** 183, (1), 180-185.

26. Larraz, G.; Orera, A.; Sanjuán, M. L., Cubic Phases of Garnet-Type $Li_7La_3Zr_2O_{12}$: the Role of Hydration. *J. Mater. Chem. A.* **2013,** 1, (37).

27. Liu, K.; Ma, J.-T.; Wang, C.-A., Excess Lithium Salt Functions More Than Compensating for Lithium Loss When Synthesizing $Li_{6.5}La_3Ta_{0.5}Zr_{1.5}O_{12}$ in Alumina Crucible. *J. Power Sources.* **2014,** 260, 109-114.

28. Yi, E.; Wang, W.; Kieffer, J.; Laine, R. M., Key Parameters Governing the Densification of Cubic- $Li_7La_3Zr_2O_{12}$ Li^+ Conductors. *J. Power Sources.* **2017,** 352, 156-164.

29. Brugge, R. H.; Hekselman, A. K. O.; Cavallaro, A.; Pesci, F. M.; Chater, R. J.; Kilner, J. A.; Aguadero, A., Garnet Electrolytes for Solid State Batteries: Visualization of Moisture-Induced Chemical Degradation and Revealing Its

Impact on the Li-Ion Dynamics. *Chem. Mater.* **2018,** 30, (11), 3704-3713.

30. Thangadurai, V.; Weppner, W., $Li_6ALa_2Ta_2O_{12}$ (A = Sr, Ba): Novel Garnet-Like Oxides for Fast Lithium Ion Conduction. *Adv. Funct. Mater.* **2005,** 15, (1), 107-112.

31. Percival, J.; Slater, P. R., Identification of the Li Sites in the Li Ion Conductor, $Li_6SrLa_2Nb_2O_{12}$, through Neutron Powder Diffraction Studies. *Solid State Commun.* **2007,** 142, (6), 355-357.

32. Percival, J.; Apperley, D.; Slater, P. R., Synthesis and Structural Characterisation of the Li Ion Conducting Garnet-Related Systems, $Li_6ALa_2Nb_2O_{12}$ (A=Ca, Sr). *Solid State Ionics.* **2008,** 179, (27-32), 1693-1696.

33. Percival, J.; Kendrick, E.; Slater, P. R., Synthesis and Characterisation of the Garnet-Related Li Ion Conductor, $Li_5Nd_3Sb_2O_{12}$. *Mater. Res. Bull.* **2008,** 43, (3), 765-770.

34. Percival, J.; Kendrick, E.; Slater, P. R., Synthesis and Conductivities of the Garnet-Related Li Ion Conductors, $Li_5Ln_3Sb_2O_{12}$ (Ln=La, Pr, Nd, Sm, Eu). *Solid State Ionics.* **2008,** 179, (27-32), 1666-1669.

35. Ohta, S.; Kobayashi, T.; Asaoka, T., High Lithium Ionic Conductivity in the Garnet-Type Oxide $Li_{7-x}La_3(Zr_{2-x}, Nb_x)O12$ (x=0–2). *J. Power Sources.* **2011,** 196, (6), 3342-3345.

36. Wolfenstine, J.; Ratchford, J.; Rangasamy, E.; Sakamoto, J.; Allen, J. L., Synthesis and High Li-ion Conductivity of Ga-Stabilized Cubic $Li_7La_3Zr_2O_{12}$. *Mater. Chem. Phys.* **2012,** 134, (2-3), 571-575.

37. Allen, J. L.; Wolfenstine, J.; Rangasamy, E.; Sakamoto, J., Effect of Substitution (Ta, Al, Ga) on the Conductivity of $Li_7La_3Zr_2O_{12}$. *J. Power Sources.* **2012,** 206, 315-319.

38. Howard, M. A.; Clemens, O.; Kendrick, E.; Knight, K. S.; Apperley, D. C.; Anderson, P. A.; Slater, P. R., Effect of Ga Incorporation on the Structure and Li Ion Conductivity of $La_3Zr_2Li_7O_{12}$. *Dalton Trans.* **2012,** 41, (39), 12048-53.

39. Li, Y.; Han, J.-T.; Wang, C.-A.; Xie, H.; Goodenough, J. B., Optimizing Li^+ Conductivity in a Garnet Framework. *J. Mater. Chem.* **2012,** 22, (30).

40. El Shinawi, H.; Janek, J., Stabilization of Cubic Lithium-Stuffed Garnets of the Type "$Li_7La_3Zr_2O_{12}$" by Addition of Gallium. *J. Power Sources.* **2013,** 225, 13-19.

41. Howard, M. A.; Clemens, O.; Knight, K. S.; Anderson, P. A.; Hafiz, S.; Panchmatia, P. M.; Slater, P. R., Synthesis, Conductivity and Structural Aspects of $Nd_3Zr_2Li_{7-3x}Al_xO_{12}$. *J. Mater. Chem. A.* **2013,** 1, (44).

42. Cheng, L.; Crumlin, E. J.; Chen, W.; Qiao, R.; Hou, H.; Franz Lux, S.; Zorba, V.; Russo, R.; Kostecki, R.; Liu, Z.; Persson, K.; Yang, W.; Cabana, J.; Richardson, T.; Chen, G.; Doeff, M., The Origin of High Electrolyte-Electrode Interfacial Resistances in Lithium Cells Containing Garnet Type Solid Electrolytes. *Phys. Chem. Chem. Phys.* **2014,** 16, (34), 18294-18300.

43. Sudo, R.; Nakata, Y.; Ishiguro, K.; Matsui, M.; Hirano, A.; Takeda, Y.; Yamamoto, O.; Imanishi, N., Interface Behavior between Garnet-Type Lithium-Conducting Solid Electrolyte and Lithium Metal. *Solid State Ionics.*

2014, 262, 151-154.

44. Aguesse, F.; Manalastas, W.; Buannic, L.; Lopez Del Amo, J. M.; Singh, G.; Llordes, A.; Kilner, J., Investigating the Dendritic Growth during Full Cell Cycling of Garnet Electrolyte in Direct Contact with Li Metal. *ACS Appl. Mater. Interfaces.* **2017,** 9, (4), 3808-3816.

45. Han, X.; Gong, Y.; Fu, K. K.; He, X.; Hitz, G. T.; Dai, J.; Pearse, A.; Liu, B.; Wang, H.; Rubloff, G.; Mo, Y.; Thangadurai, V.; Wachsman, E. D.; Hu, L., Negating Interfacial Impedance in Garnet-Based Solid-State Li Metal Batteries. *Nat. Mater.* **2017,** 16, (5), 572-579.

46. Dai, J.; Yang, C.; Wang, C.; Pastel, G.; Hu, L., Interface Engineering for Garnet-Based Solid-State Lithium-Metal Batteries: Materials, Structures, and Characterization. *Adv. Mater.* **2018,** 30, (48), e1802068.

47. Li, Y.; Chen, X.; Dolocan, A.; Cui, Z.; Xin, S.; Xue, L.; Xu, H.; Park, K.; Goodenough, J. B., Garnet Electrolyte with an Ultralow Interfacial Resistance for Li-Metal Batteries. *J. Am. Chem. Soc.* **2018,** 140, (20), 6448-6455.

48. Zhou, W.; Wang, Z.; Pu, Y.; Li, Y.; Xin, S.; Li, X.; Chen, J.; Goodenough, J. B., Double-Layer Polymer Electrolyte for High-Voltage All-Solid-State Rechargeable Batteries. *Adv. Mater.* **2019,** 31, (4), e1805574.

49. Zhang, W.; Nie, J.; Li, F.; Wang, Z. L.; Sun, C., A Durable and Safe Solid-State Lithium Battery with a Hybrid Electrolyte Membrane. *Nano Energy.* **2018,** 45, 413-419.

50. Dong, B.; Yeandel, S. R.; Goddard, P.; Slater, P. R., Combined

Experimental and Computational Study of Ce-Doped $La_3Zr_2Li_7O_{12}$ Garnet Solid-State Electrolyte. *Chem. Mater.* **2019,** 32, (1), 215-223.

51. Kotobuki, M.; Koishi, M., Preparation of $Li_7La_3Zr_2O_{12}$ Solid Electrolyte via A Sol–Gel Method. *Ceram. Int.* **2014,** 40, (3), 5043-5047.

52. Kumar, P. J.; Nishimura, K.; Senna, M.; Düvel, A.; Heitjans, P.; Kawaguchi, T.; Sakamoto, N.; Wakiya, N.; Suzuki, H., A Novel Low-Temperature Solid-State Route for Nanostructured Cubic Garnet $Li_7La_3Zr_2O_{12}$ and Its Application to Li-Ion Battery. *RSC Adv.* **2016,** 6, (67), 62656-62667.

53. Yang, T.; Zheng, J.; Cheng, Q.; Hu, Y. Y.; Chan, C. K., Composite Polymer Electrolytes with $Li_7La_3Zr_2O_{12}$ Garnet-Type Nanowires as Ceramic Fillers: Mechanism of Conductivity Enhancement and Role of Doping and Morphology. *ACS Appl. Mater. Interfaces* **2017,** 9, (26), 21773-21780.

54. Paulus, A.; Kammler, S.; Heuer, S.; Paulus, M. C.; Jakes, P.; Granwehr, J.; Eichel, R.-A., Sol Gel vs Solid State Synthesis of the Fast Lithium-Ion Conducting Solid State Electrolyte $Li_7La_3Zr_2O_{12}$ Substituted with Iron. *J. Electrochem. Soc.* **2019,** 166, (3), A5403-A5409.

55. Danks, A. E.; Hall, S. R.; Schnepp, Z., The Evolution of 'Sol–Gel' Chemistry as A Technique for Materials Synthesis. *Mater. Horiz.* **2016,** 3, (2), 91-112.

56. Zilinskaite, S.; Rennie, A. J. R.; Boston, R.; Reeves-McLaren, N., Biotemplating: a Sustainable Synthetic Methodology for Na-Ion Battery Materials. *J. Mater. Chem. A.* **2018,** 6, (13), 5346-5355.

57. Li, Y.; Xu, B.; Xu, H.; Duan, H.; Lu, X.; Xin, S.; Zhou, W.; Xue, L.; Fu, G.; Manthiram, A.; Goodenough, J. B., Hybrid Polymer/Garnet Electrolyte with a Small Interfacial Resistance for Lithium-Ion Batteries. *Angew. Chem. Int. Ed.* **2017,** 56, (3), 753-756.

58. Smetaczek, S.; Wachter-Welzl, A.; Wagner, R.; Rettenwander, D.; Amthauer, G.; Andrejs, L.; Taibl, S.; Limbeck, A.; Fleig, J., Local Li-Ion Conductivity Changes Within Al Stabilized $Li_7La_3Zr_2O_{12}$ and Their Relationship to Three-Dimensional Variations of the Bulk Composition. *J. Mater. Chem. A.* **2019,** 7, (12), 6818-6831.

59. Wachter-Welzl, A.; Kirowitz, J.; Wagner, R.; Smetaczek, S.; Brunauer, G. C.; Bonta, M.; Rettenwander, D.; Taibl, S.; Limbeck, A.; Amthauer, G.; Fleig, J., The Origin of Conductivity Variations in Al-Stabilized $Li_7La_3Zr_2O_{12}$ Ceramics. *Solid State Ionics.* **2018,** 319, 203-208.

60. Liu, Y.; Sun, Q.; Wang, D.; Adair, K.; Liang, J.; Sun, X., Development of the Cold Sintering Process and Its Application in Solid-State Lithium Batteries. *J. of Power Sources.* **2018,** 393, 193-203.

61. Irvine, J. T. S.; Sinclair, D. C.; West, A. R., Electroceramics: Characterization by Impedance Spectroscopy. *Adv. Mater.* **1990,** 2, 132.

62. Dong, B.; Hull, S.; West, A. R., Phase Formation, Crystallography, and Ionic Conductivity of Lithium Manganese Orthosilicates. *Inorg. Chem.* **2019,** 58, (1), 715-723.

Caption of figures

Fig 1 The structure of Agar.

Fig 2 (a) XRD patterns of $Li_7La_3Zr_2O_{12}$ synthesised with or without Agar. (b) XRD patterns of $Li_7La_3Zr_2O_{12}$ synthesised using 0.1M, 0.25M, 0.5M and 1M dilute nitric acid. (c) SEM images of $Li_{6.4}Al_{0.2}La_3Zr_2O_{12}$ prepared from solid state and Agar biotemplate route at 700 ^oC.

Fig 3 (a) VT-XRD of $Li_7La_3Zr_2O_{12}$ made from 300 to 800 ^oC.

Fig 4 (a) XRD patterns of $Li_7La_3Zr_2O_{12}$ and $Li_{6.4}Al_{0.2}La_3Zr_2O_{12}$ made at 700 °C using biopolymer sol gel route. (b) SEM and EDX mapping of $Li_{6.4}Al_{0.2}La_3Zr_2O_{12}$.

Fig 5 XRD patterns of $Li_{6.55}Al_{0.15}La_3Zr_2O_{12}$ without (cubic phase due to Al incorporation) and with 10% excess Li (tetragonal phase, suggesting negligible Al incorporation) made at 700 ^oC.

Fig 6 Impedance data of LiF-$Li_{6.4}Al_{0.2}La_3Zr_2O_{12}$. (a) Fitted and experimental

complex Z* data (b) Spectroscopic plot of C' (c) Spectroscopic plot of Y'

Fig 7 Arrhenius plot of LiF-$Li_{6.4}Al_{0.2}La_3Zr_2O_{12}$.

Table 1 Comparison of the synthesis routes of $Li_7La_3Zr_2O_{12}$.

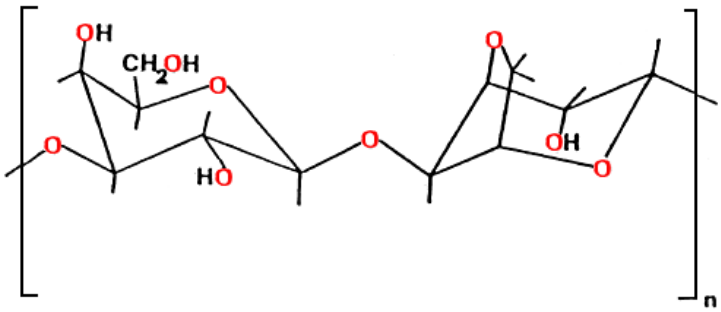

Fig 1

(a)

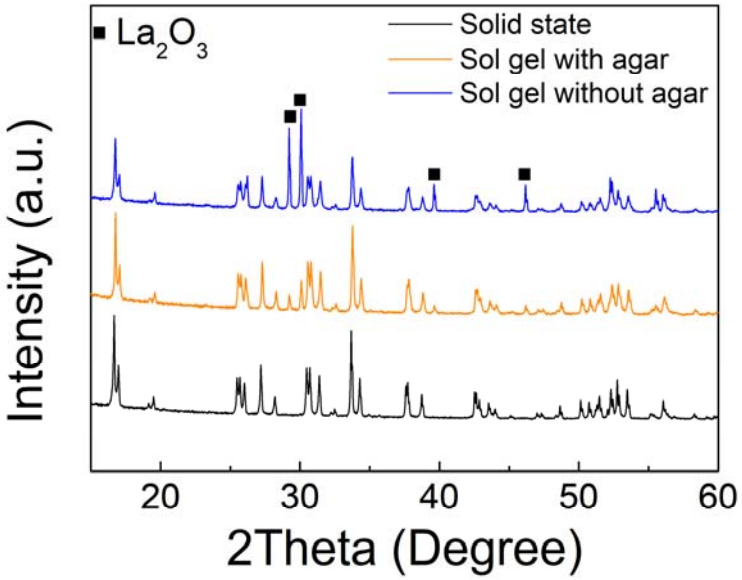
■ La2O3
Solid state
Sol gel with agar
Sol gel without agar
Intensity (a.u.)
20
30
40
50
60
2Theta (Degree)

(b)

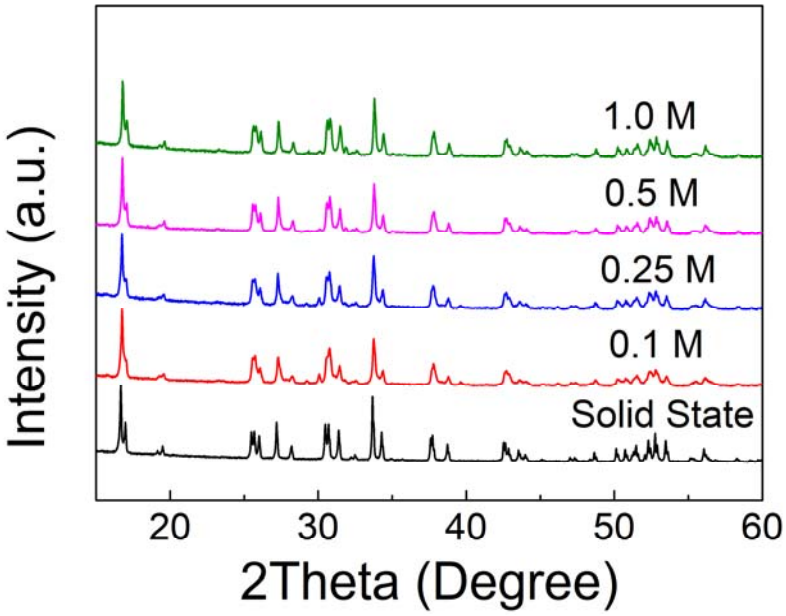
1.0 M
0.5 M
0.25 M
0.1 M
Solid State
Intensity (a.u.)
20
30
40
50
60
2Theta (Degree)

(c)

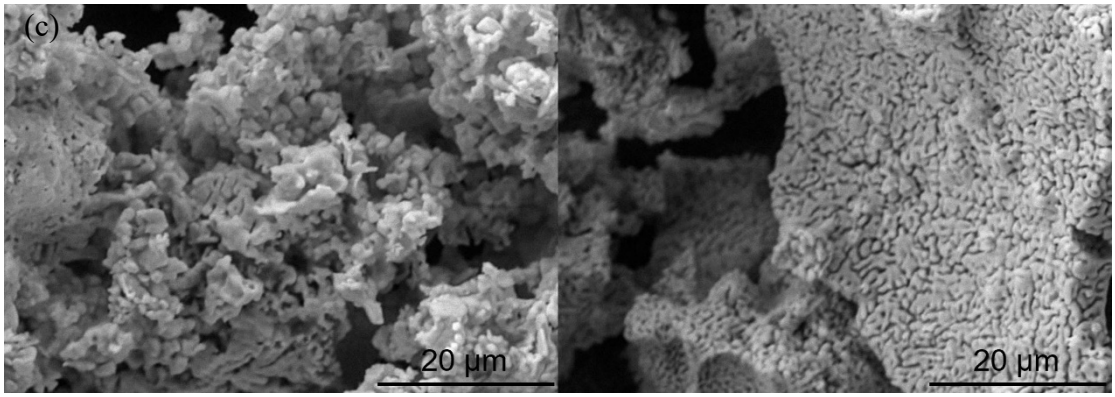
20 μm
20 μm

Fig 2

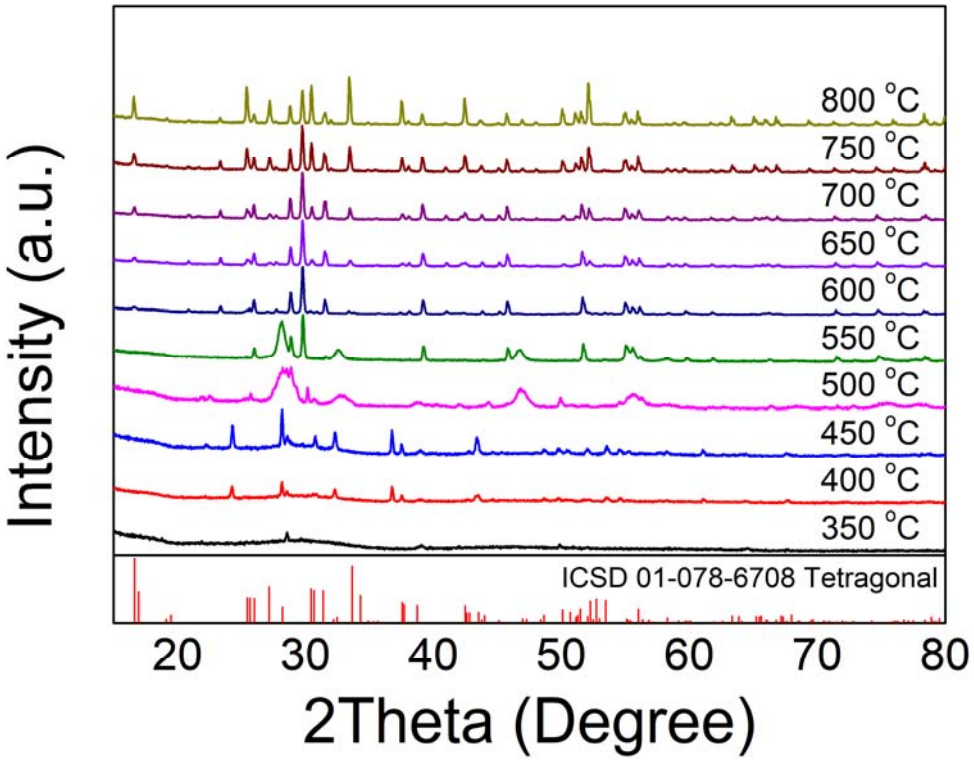
Intensity (a.u.)
800 °C
750 °C
700 °C
650 °C
600 °C
550 °C
500 °C
450 °C
400 °C
350 °C
ICSD 01-078-6708 Tetragonal
20
30
40
50
60
70
80
2Theta (Degree)

Fig 3

(a)

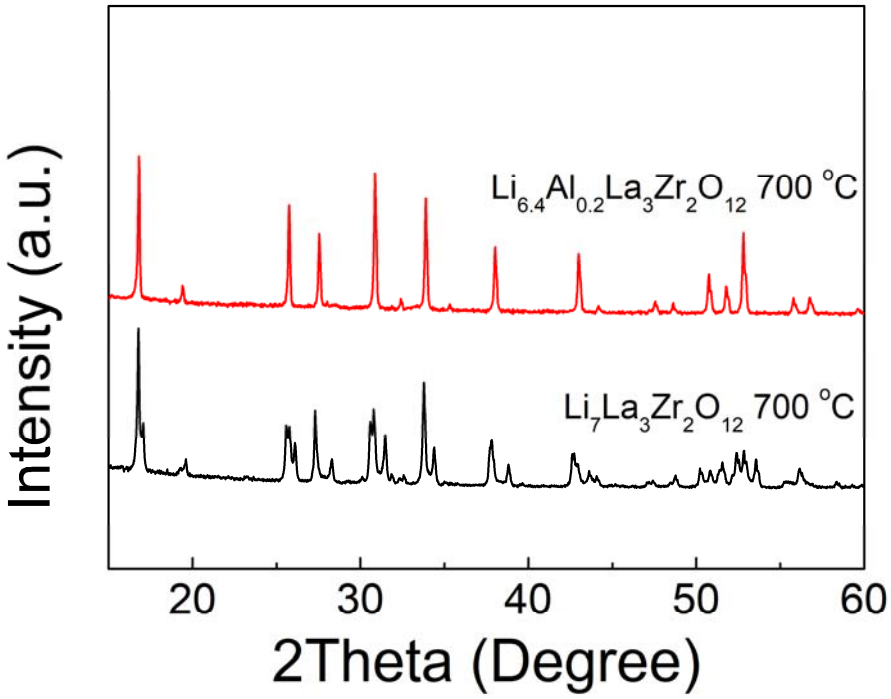
Intensity (a.u.)
Li6.4Al0.2La3Zr2O12 700 °C
Li7La3Zr2O12 700 °C
20
30
40
50
60
2Theta (Degree)

(b)

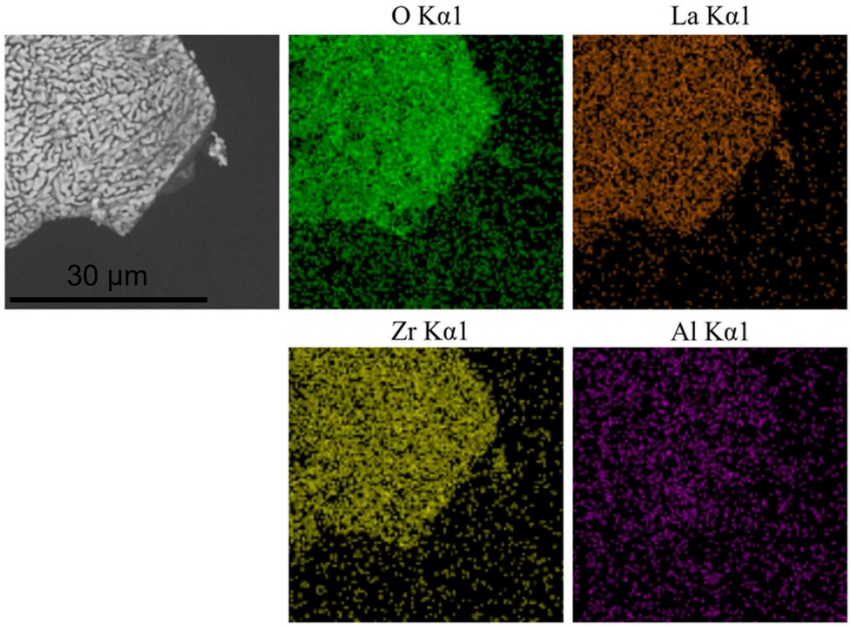
30 μm
O Kα1
La Kα1
Zr Kα1
Al Kα1

Fig 4

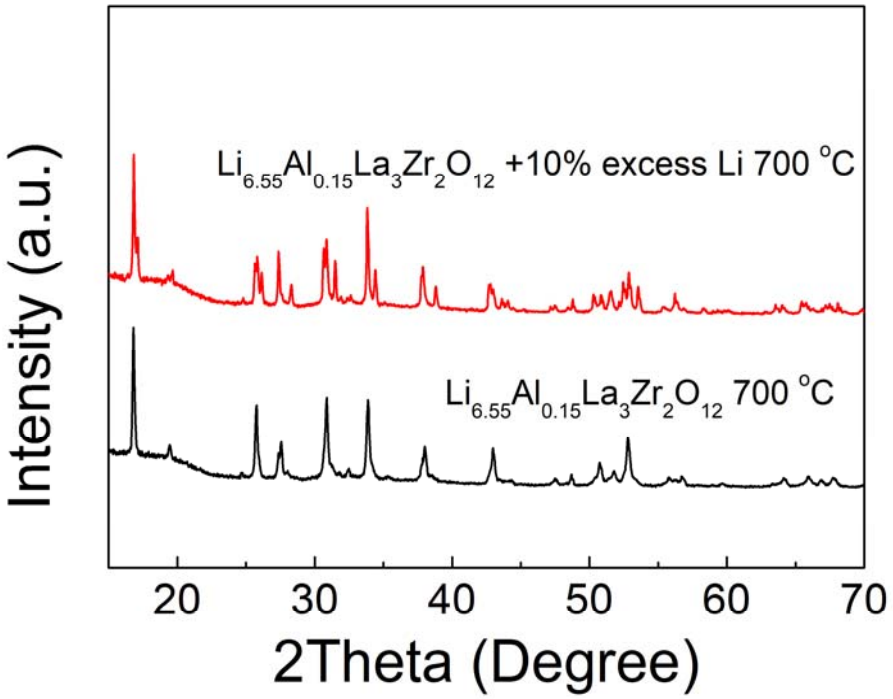
Li6.55Al0.15La3Zr2O12 +10% excess Li 700 °C
Li6.55Al0.15La3Zr2O12 700 °C
Intensity (a.u.)
20
30
40
50
60
70
2Theta (Degree)

Fig 5

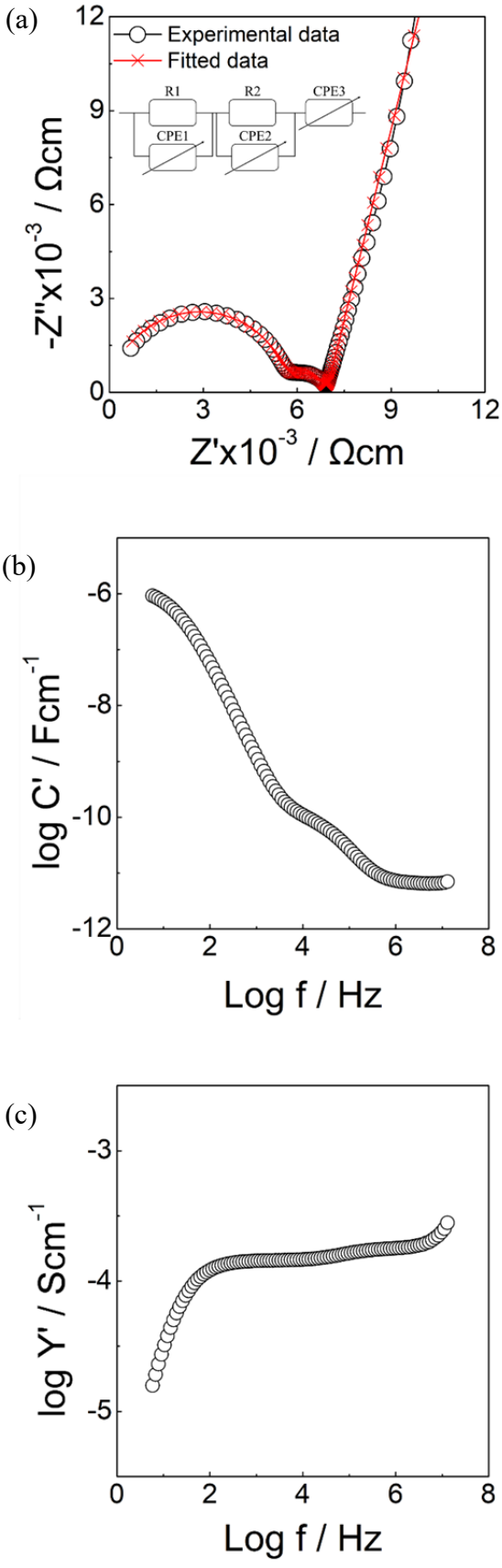
(a)
Experimental data
Fitted data
R1
R2
CPE3
CPE1
CPE2
-Z''x10^-3 / Ωcm
Z'x10^-3 / Ωcm
0
3
6
9
12
(b)
log C' / Fcm^-1
Log f / Hz
-6
-8
-10
-12
0
2
4
6
8
(c)
log Y' / Scm^-1
Log f / Hz
-3
-4
-5
0
2
4
6
8

Fig 6

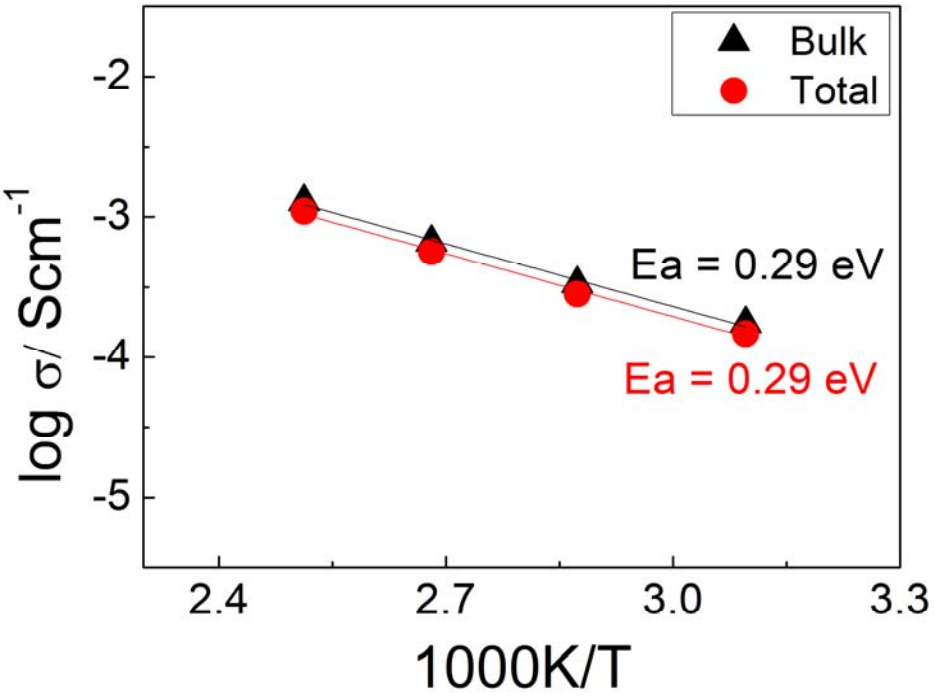

Fig 7

Table 1

Method	Starting Materials	Temperature	Final Product
Solid State[22]	LiOH, La_2O_3, ZrO_2	1230 ^oC/36h	$Li_7La_3Zr_2O_{12}$
Sol-gel[51]	CH_3COOLi, $La(CH_3COO)_3 \cdot 1.5H_2O$, $Zr(C_4H_9O)_4$, CH_3COOH, C_3H_7OH,	1000 - 1100 ^oC/6h	$Li_7La_3Zr_2O_{12}$ and $La_2Zr_2O_7$
Biotemplating (this work)	$La(NO_3)_3 \cdot 6H_2O$, $ZrO(NO_3)_2 \cdot xH_2O$, $LiNO_3$, Agar	700 ^oC/12h	$Li_7La_3Zr_2O_{12}$

Supporting Information

Low Temperature Synthesis of Garnet Solid State Electrolytes: Implications on Aluminium Incorporation in $Li_7La_3Zr_2O_{12}$

Bo Dong[†,], Laura L. Driscoll[†], Mark P. Stockham[†], Emma Kendrick[‡], Peter R. Slater[†,*]*

†School of Chemistry, University of Birmingham, B15 2TT, UK

‡School of Metallurgy and Materials, University of Birmingham, B15 2TT, UK

*b.dong@bham.ac.uk; p.r.slater@bham.ac.uk;

Structure refinement

For $Li_7La_3Zr_2O_{12}$ [1], U_{isos} of Li1, Al1, La2, Al2, O1, O2, O3 were set to 0.025 $Å^2$. The scale factor, background and lattice parameters were refined, followed by peak profile coefficient and zero, which were fixed after convergency. At last. atomic coordinates of La2, U_{isos} of La1, Zr1, La2 were refined together. For $Li_{6.4}Al_{0.2}La_3Zr_2O_{12}$, U_{isos} of Li1, Al1, La2, Al2 were set to 0.025 $Å^2$, and occupancies of Al1, Li1 and L2 were were scaled up from published occupancies to ensure ensure the charge-neutrality [2]. The scale factor, background and lattice parameters were refined, followed by peak profile coefficient and zero, which were fixed after convergency. At last. atomic coordinates of O1, U_{isos} of La1, Zr1, O1 were refined together. The refined parameters were shown in table S1 and S2.

Similar refinement strategies were applied to those of $Li_{6.55}Al_{0.15}La_3Zr_2O_{12}$ with or without 10% excess Li. The refined parameters were shown in table S3 and S4.

Electrochemical properties

The electrochemical impedance complex plane of Li//$Li_{6.4}Al_{0.2}La_3Zr_2O_{12}$//Li cell at 55 ^oC is shown in figure S5(a). Two parallel resistor and capacitor in series, which represent the total and interfacial resistances, were used to fit the circuit. A total resistance of 1208 Ωcm^2 and an interfacial resistance of 48 Ωcm^2 were seen in the cell. Long term plating/stripping curves of the Li//$Li_{6.4}Al_{0.2}La_3Zr_2O_{12}$//Li cell at 55 ^oC is shown in figure S5(b). A flat plate with a

overpotential voltage of 50 mV is seen at 50 μAcm^{-2} current density. While a slight voltage hysteresis is observed at the higher current density of 100 μAcm^{-2}, the long-term cycling stability over 210 hours was still delivered.

References

[1] Awaka J., Kijima N., Hayakawa H., Akimoto J., Synthesis and structure analysis of tetragonal $Li_7La_3Zr_2O_{12}$ with the garnet-related type structure, J. Solid State Chem. 182 (8) (2009) 2046–2052.

[2] Chen Y., Rangasamy E., Liang C.D., An, K., Origin of high Li^+ conduction in doped $Li_7La_3Zr_2O_{12}$ garnets. Chem. Mater. 27 (16) (2015) 5491-5494.

Captions of figures and tables

Fig S1. Observed, calculated and difference profiles from Rietveld refinement for $Li_7La_3Zr_2O_{12}$ using XRD data.

Table S1. Refined structural parameters for $Li_7La_3Zr_2O_{12}$ using XRD data.

Fig S2. Observed, calculated and difference profiles from Rietveld refinement for $Li_{6.4}Al_{0.2}La_3Zr_2O_{12}$ using XRD data.

Table S2. Refined structural parameters for $Li_{6.4}Al_{0.2}La_3Zr_2O_{12}$ using XRD data.

Fig S3. Observed, calculated and difference profiles from Rietveld refinement for $Li_{6.55}Al_{0.15}La_3Zr_2O_{12}$ using XRD data.

Table S3. Refined structural parameters for $Li_{6.55}Al_{0.15}La_3Zr_2O_{12}$ using XRD data.

Fig S4. Observed, calculated and difference profiles from Rietveld refinement for $Li_{6.55}Al_{0.15}La_3Zr_2O_{12}$ with 10% excess Li using XRD data.

Table S4. Refined structural parameters for $Li_{6.55}Al_{0.15}La_3Zr_2O_{12}$ with 10% excess Li using XRD data.

Fig S5. (a) Impedance spectra of Li//$Li_{6.4}Al_{0.2}La_3Zr_2O_{12}$//Li symmetric cell. (b) Charge – discharge voltage profile of Li//$Li_{6.4}Al_{0.2}La_3Zr_2O_{12}$//Li symmetry cell at 55 ^oC with 25, 50 and 100 μA cm^{-2} current densities.

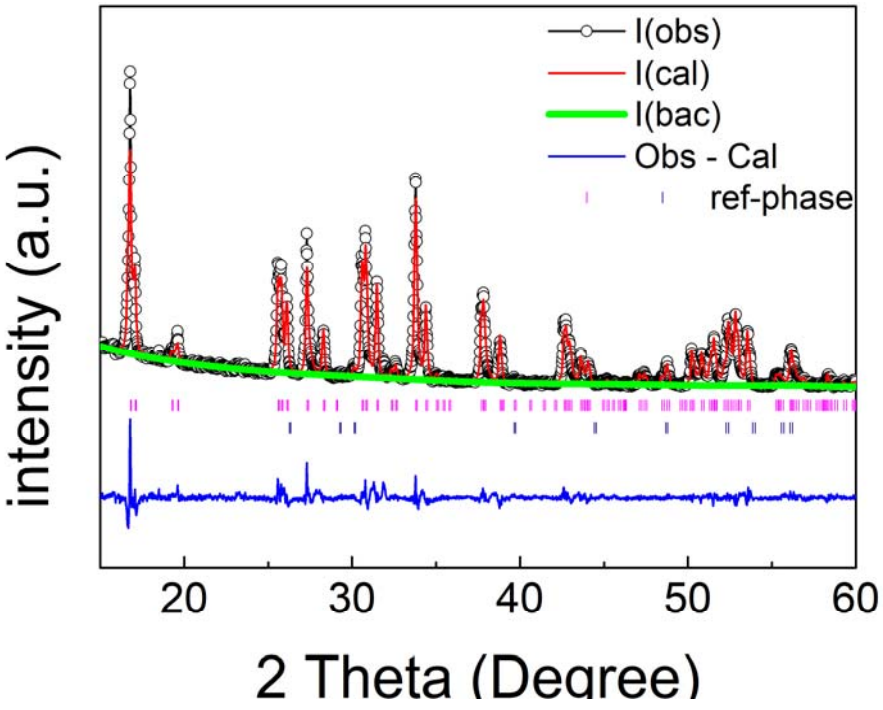

Fig S1

Table S1

Atom	*x*	*y*	*z*	Mult.	Occupancy	$u_{iso}\times100$ (Å^2)
La1	0	0.25	0.125	8	1	0.8(3)
La2	0.1273(4)	0	0.25	16	1	0.5(2)
Zr1	0	0	0	16	1	1.2(2)
Li1	0	0.25	0.375	8	1	2.5
Li2	0.1774	0.4274	0.125	16	1	2.5
Li3	0.08	0.087	0.8049	32	1	2.5
O1	-0.034	0.0551	0.1517	32	1	2.5
O2	0.0543	0.8519	0.5334	32	1	2.5
O3	0.1491	0.0281	0.4464	32	1	2.5

a = 13.1245(4)Å, *b* = 13.1245(4)Å, *c* = 12.6894(6)Å, V = 2139.94(8) Å^3

χ^2 = 6.528, R_{wp} = 12.57, R_p = 9.77%

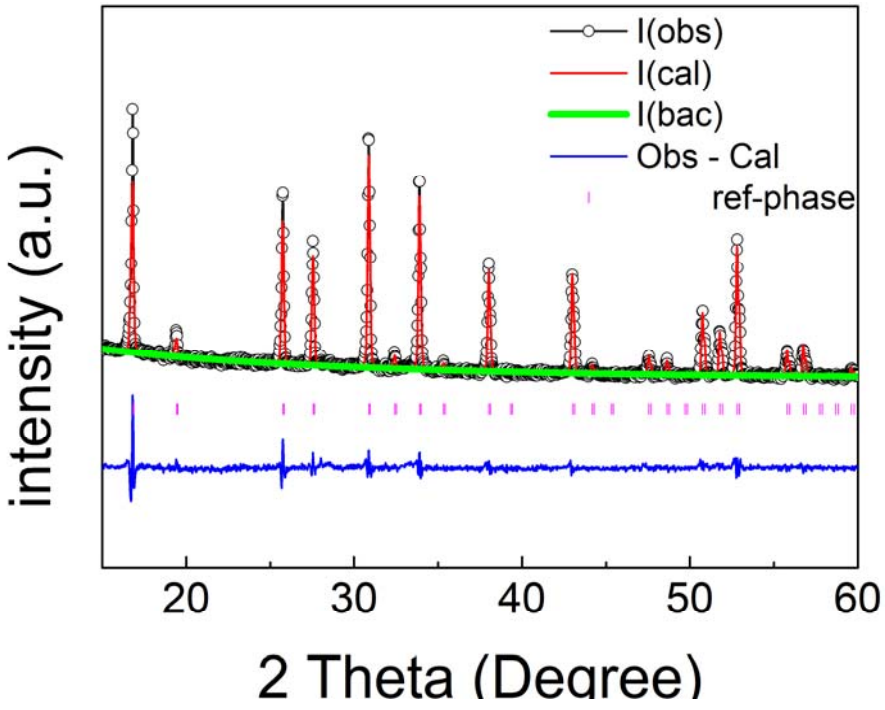

Fig S2

Table S2

Atom	*x*	*y*	*z*	Mult.	Occupancy	$u_{iso}\times100$ (Å^2)
La1	0.125	0	0.25	24	1	1.2(1)
Zr1	0	0	0	16	1	0.8(2)
O1	0.1005(4)	0.1923(5)	0.2835(5)	96	1	2.3(5)
Li1	0.375	0	0.25	24	0.675	2.5
Al1	0.375	0	0.25	24	0.067	2.5
Li2	0.1018	0.187	0.4222	96	0.365	2.5

a = 12.9939(2)Å, V = 2139.94(8) Å^3

χ^2 = 3.339, R_{wp} = 10.35, R_p = 7.07%

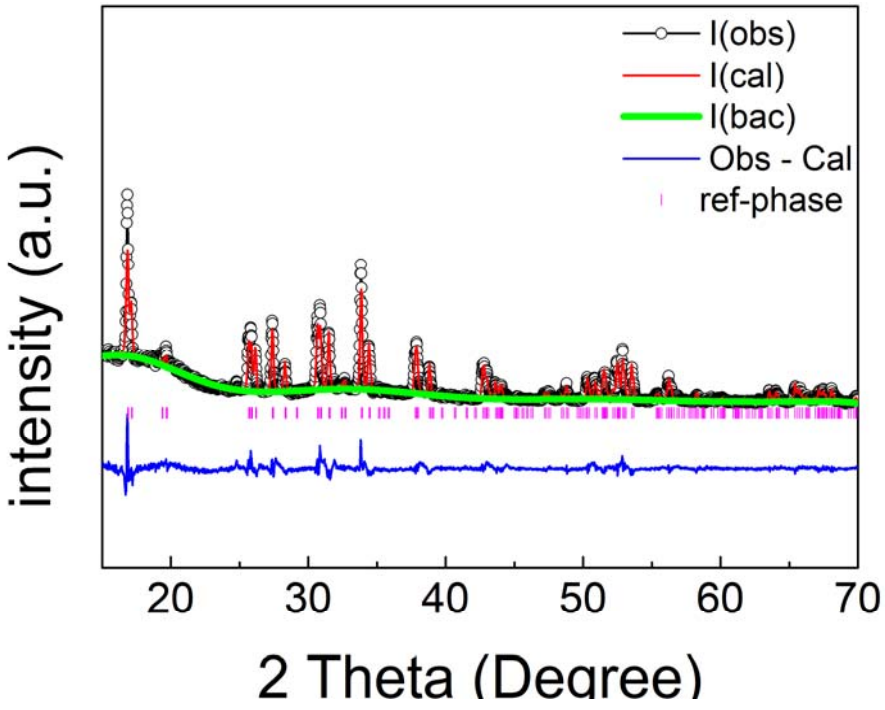

Fig S3

Table S3

Atom	*x*	*y*	*z*	Mult.	Occupancy	$u_{iso}\times100$ ($Å^2$)
La1	0.125	0	0.25	24	1	1.0(2)
Zr1	0	0	0	16	1	0.3(2)
O1	0.1044(4)	0.1855(11)	0.2829(9)	96	1	3.7(7)
Li1	0.375	15	0.25	24	0.691	2.5
Al1	0.375	0	0.25	24	0.05	2.5
Li2	0.1018	0.187	0.4222	96	0.373	2.5
a = 13.0089(4)Å, V = 2201.5(2) $Å^3$						
χ^2 = 6.023, R_{wp} = 12.3%, R_p = 9.23%						

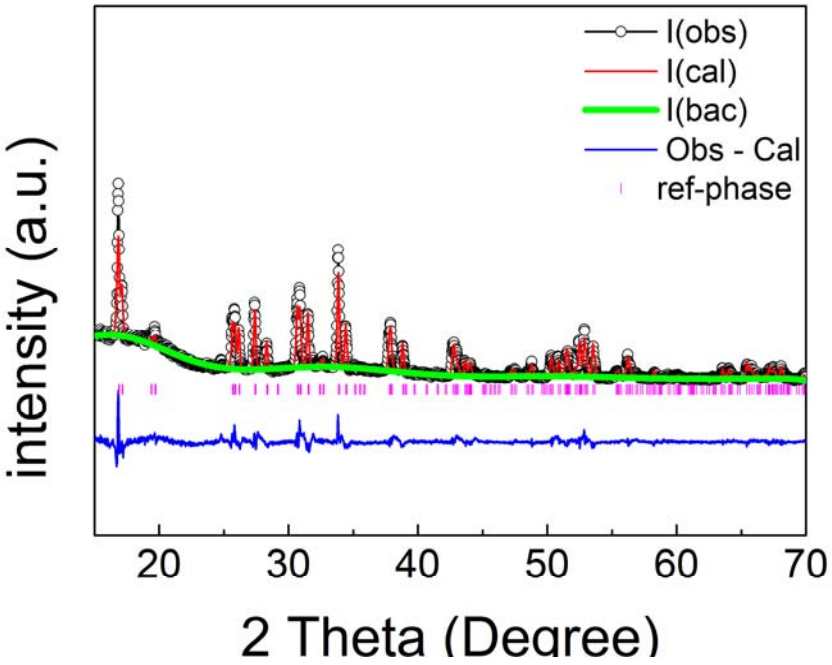

Fig S4

Table S4

Atom	*x*	*y*	*z*	Mult.	Occupancy	$u_{iso}\times100$ (Å^2)
La1	0	0.25	0.125	8	1	1.0(3)
La2	0.1279(4)	0	0.25	16	1	0.1(2)
Zr1	0	0	0	16	1	1.1(2)
Li1	0	0.25	0.375	8	1	2.5
Li2	0.1774	0.4274	0.125	16	1	2.5
Li3	0.08	0.087	0.8049	32	1	2.5
O1	-0.034	0.0551	0.1517	32	1	2.5
O2	0.0543	0.8519	0.5334	32	1	2.5
O3	0.1491	0.0281	0.4464	32	1	2.5

a = 13.1284(3)Å, *b* = 13.1284(3)Å, *c* = 12.7117(5)Å, V = 2190.93(11) Å^3

χ^2 = 4.961, R_{wp} = 12.65, R_p = 10.38%

(a)

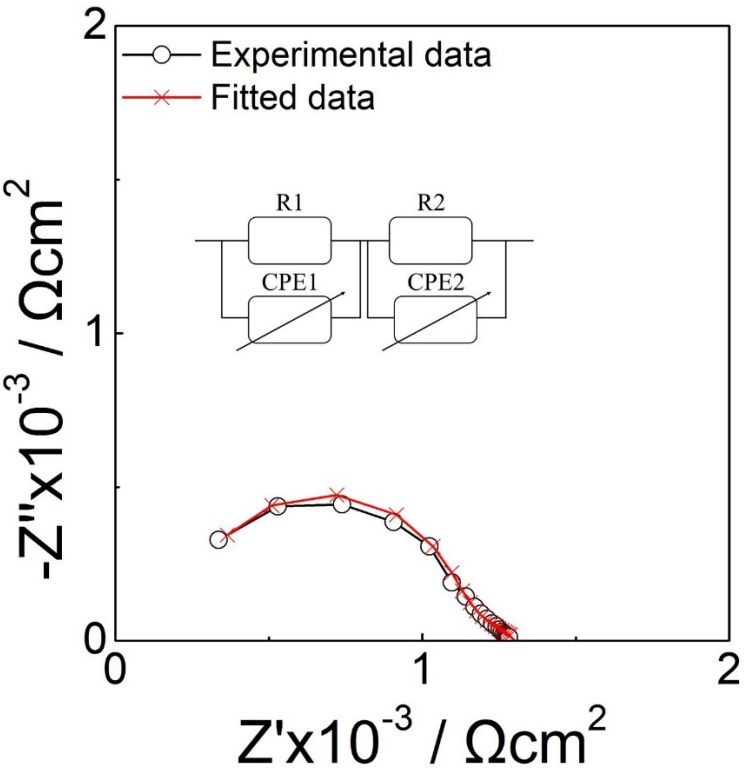
Experimental data
Fitted data
R1
R2
CPE1
CPE2
-Z''x10-3 / Ωcm2
Z'x10-3 / Ωcm2
0
1
2

(b)

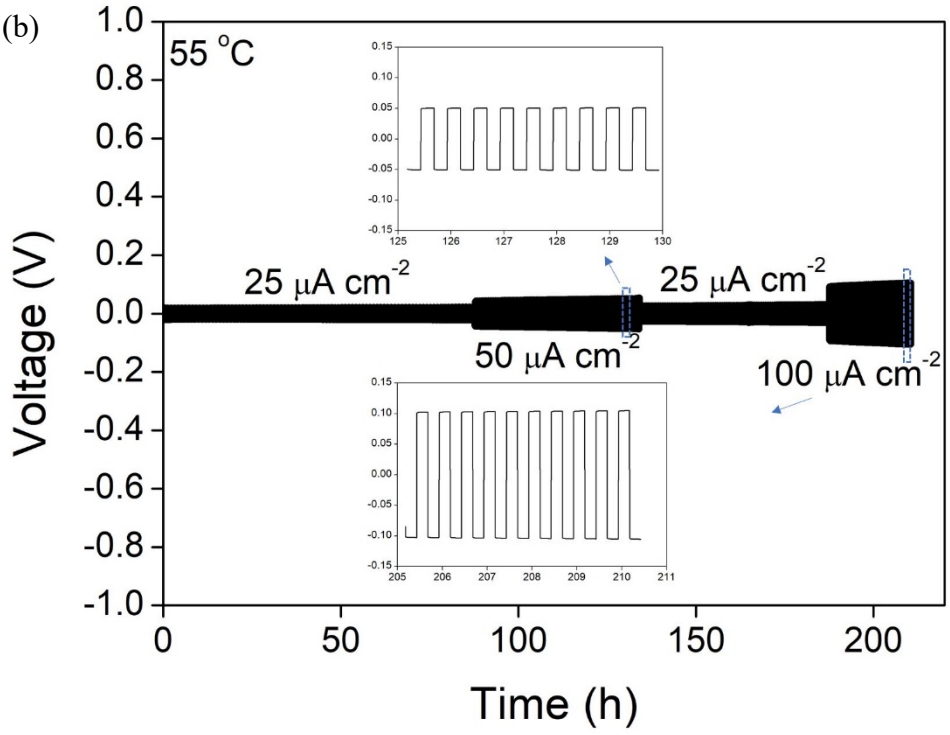
55 °C
25 μA cm-2
50 μA cm-2
25 μA cm-2
100 μA cm-2
Voltage (V)
Time (h)

Fig S5